Dynamics of classical particles in oval or elliptic billiards with a dispersing mechanism

Diogo Ricardo da Costa, Carl P. Dettmann, Juliano A. de Oliveira, and Edson D. Leonel

Citation: Chaos: An Interdisciplinary Journal of Nonlinear Science **25**, 033109 (2015); doi: 10.1063/1.4915474
View online: http://dx.doi.org/10.1063/1.4915474
View Table of Contents: http://scitation.aip.org/content/aip/journal/chaos/25/3?ver=pdfcov
Published by the AIP Publishing

Dynamics of classical particles in oval or elliptic billiards with a dispersing mechanism

Diogo Ricardo da Costa,[1,2,3] Carl P. Dettmann,[2] Juliano A. de Oliveira,[4] and Edson D. Leonel[3]
[1]*Instituto de Física da USP, Rua do Matão, Travessa R, 187, Cidade Universitária, CEP 05314-970 São Paulo, SP, Brazil*
[2]*School of Mathematics, University of Bristol, Bristol, United Kingdom*
[3]*Departamento de Física, UNESP-Univ Estadual Paulista, Av. 24A, 1515, 13506-900 Rio Claro, SP, Brazil*
[4]*UNESP-Univ Estadual Paulista, Câmpus de São João da Boa Vista, São João da Boa Vista, SP, Brazil*

(Received 11 December 2014; accepted 9 March 2015; published online 20 March 2015)

Some dynamical properties for an oval billiard with a scatterer in its interior are studied. The dynamics consists of a classical particle colliding between an inner circle and an external boundary given by an oval, elliptical, or circle shapes, exploring for the first time some natural generalizations. The billiard is indeed a generalization of the annular billiard, which is of strong interest for understanding marginally unstable periodic orbits and their role in the boundary between regular and chaotic regions in both classical and quantum (including experimental) systems. For the oval billiard, which has a mixed phase space, the presence of an obstacle is an interesting addition. We demonstrate, with details, how to obtain the equations of the mapping, and the changes in the phase space are discussed. We study the linear stability of some fixed points and show both analytically and numerically the occurrence of direct and inverse parabolic bifurcations. Lyapunov exponents and generalized bifurcation diagrams are obtained. Moreover, histograms of the number of successive iterations for orbits that stay in a cusp are studied. These histograms are shown to be scaling invariant when changing the radius of the scatterer, and they have a power law slope around −3. The results here can be generalized to other kinds of external boundaries. © *2015 AIP Publishing LLC*. [http://dx.doi.org/10.1063/1.4915474]

A billiard consists in the dynamics of a point particle moving freely in a closed region and suffering specular collisions with the boundaries. In this paper, a billiard with a circular scatterer in its interior is studied, while three shapes are considered for the outer boundary: oval, elliptical, or circle shapes, as a generalization of annular billiard. The equations of the mapping are constructed with details. Depending on the control parameters, the phase space presents a mixed structure, having periodic islands, chaotic seas, and invariant spanning curves. The linear stability of some fixed point is studied showing the occurrence of direct and inverse parabolic bifurcations. Generalized bifurcation diagrams are also studied, which utilizes an important tool to characterize chaotic regions called Lyapunov exponents. Histograms for the number of successive iterations for orbits that stay in a cusp are studied. The histograms are shown to be scaling invariant with respect to the radius of the inner circle. These cusps can create singularities in the billiard and they are object of study for many different problems.

I. INTRODUCTION

Billiard problems have been widely studied in the last years.[1–5] They were introduced in the 1920s by Birkhoff[6] and consist of closed domains in which a point like particle collides and suffers specular reflections with the boundaries. Birkhoff's idea was to have a simple class of models, which shows the complicated behavior of non-integrable smooth Hamiltonian systems without the need to integrate a differential equation.[6,7] By connecting the dynamics with geometry, billiards serve as models to address numerous systems. One example includes the foundations of the ergodic hypothesis.[8,9] Different applications can be found in the literature, and both classical and quantum[2] cases are observed. It is possible, for example, to study the dynamics of a dissipative, inelastic gravitational billiard,[10] the ray chaos in an architectural acoustic semi-stadium system billiard,[11] photon neutralizer as an example of an open billiard,[12] and many other applications.[13–17]

In this paper, we consider a generalization for the annular billiard[18–21] consisting of a particle colliding between an inner circle and an external boundary given by an oval, elliptic, or circle shapes. Annular billiards have many applications in the literature, for example, they are of strong interest for understanding MUPOs (marginally unstable periodic orbits) and their role in the boundary between regular and chaotic regions in both classical and quantum (including experimental) systems. These MUPOs are not structurally stable and may be destroyed if a small perturbation is applied in the parameters of the system. It was assumed that they can only exist for special systems, like billiard with parallel walls, but contradicting this, in Ref. 8, it was observed that MUPOs are prevalent in a large class of billiard systems. Another applications involving annular billiards can be found when studying annular microwave billiards, where the first experimental evidence for chaos-assisted tunneling was

found.[22,23] Many billiards contain a mixed phase space, which have periodic islands commonly surrounded by a chaotic sea, and invariant spanning curves, limiting the *size* of the chaotic sea. Examples of integrable billiards are circular or elliptical billiard,[24] where for this last one, the integrability comes from the conservation of product of angular momenta with respect to the two foci.[25]

It is important to remember that for the billiard presented in Ref. 18, the mechanism that generated chaos is the focusing-dispersing, but even if we do not use an internal boundary in our billiard, the chaos can appears only changing the parameter that describe the boundary of the oval billiard.

Here, some special orbits are studied as well as their linear stability obtained as an attempt to show the occurrence of direct or inverse parabolic bifurcations. The direct parabolic bifurcation generically means the creation of periodic orbits in a saddle-center bifurcation. For the inverse parabolic bifurcation, the periodic orbit depends continuously on the bifurcation parameter, and this is the most important difference compared with the direct parabolic case,[7] and in such a case a period doubling bifurcation is observed. We obtained the Lyapunov exponents and presented some conservative generalized bifurcation diagrams (CGBD).[26] These diagrams are important because they show the very complex, self-similar, and generic bifurcation structure in conservative systems with only one parameter and they are used to recognize the bifurcation diagram in conservative systems in a simple way.[26] Also we study a special situation, where the scatterer touches the external boundary and creates a cusp. In such a situation, we note that some orbits can enter in this region, and changes in some observables are observed. For example, the histogram for the number of successive iterations in this region has a power law with slope around -3. These histograms are shown to be scaling invariant when the radius of the internal circle is changed. The cusps can create singularities in the billiard and they are object of study for different problems.[27,28] For example, it is possible to study the decay of correlations and invariance principles for dispersing billiards with cusps and related planar billiard flows.[29] In the literature, it is possible to observe only cusps with two dispersing or one dispersing and one flat boundary.[27–29]

This paper is organized as follows: in Sec. II, the model, the map, and numerical results are presented. The summary and conclusions are shown in Sec. III.

II. THE MODEL, THE MAP, AND NUMERICAL RESULTS

In this section, we present all the necessary details to construct the mapping that describes the dynamics of the system. To start with, we consider the model of a classical particle confined inside and experiencing collisions with an oval, elliptic, or circle billiard. Later, we introduce in the interior of the billiard a circle, working as a scatterer. The dynamics of the particle is described in terms of a two-dimensional non-linear mapping $T(\theta_n, \alpha_n) = (\theta_{n+1}, \alpha_{n+1})$, where the variables denote: (θ) the angular position of the particle and (α) the angle that the trajectory of the particle forms with the tangent line at the position of the collision. Fig. 1 illustrates the dynamics for a particle hitting the internal circle after colliding with the external boundary. The velocity between collisions is constant because the boundary is static and no forces are acting on the during the particle flight. The shape of the oval billiard in polar coordinates is given by

$$R(\theta, p, \epsilon) = 1 + \epsilon \cos[p\theta], \tag{1}$$

where $\epsilon \in [0, 1)$ is the parameter which controls the deformation of the boundary and p is a positive integer number. If $\epsilon = 0$, the circular billiard is recovered. For $\epsilon > \epsilon_c = \frac{1}{1+p^2}$,[30] some negative local curvatures as shown in Fig. 1 for $p = 2$ and $\epsilon = 0.3 > \epsilon_c$ (in such a situation $\epsilon_c = 0.2$) are observed.

For the elliptical billiard, the boundary shape is given by

$$R(\theta, a, b) = \frac{ab}{\sqrt{[b\cos(\theta)]^2 + [a\sin(\theta)]^2}}, \tag{2}$$

where a and b are, respectively, one-half of the ellipse's major and minor axes. If $a = b > 0$, the circle billiard is recovered.

The Cartesian components of the boundary are given by

$$X(\theta) = R(\theta)\cos(\theta), \tag{3}$$

$$Y(\theta) = R(\theta)\sin(\theta)\,. \tag{4}$$

Starting with an initial condition (θ_n, α_n), the angle between the tangent at the boundary and the horizontal axis at the point $X(\theta_n)$ and $Y(\theta_n)$ is given by $\phi_n = \arctan[Y'(\theta_n)/X'(\theta_n)]$, where

$$X'(\theta_n) = dX/d\theta_n = \frac{\mathrm{d}R(\theta_n)}{\mathrm{d}\theta_n}\cos(\theta_n) - R(\theta_n)\sin(\theta_n) \tag{5}$$

and

$$Y'(\theta_n) = dY/d\theta_n = \frac{\mathrm{d}R(\theta_n)}{\mathrm{d}\theta_n}\sin(\theta_n) + R(\theta_n)\cos(\theta_n), \tag{6}$$

where for the oval billiard we have

$$\frac{\mathrm{d}R(\theta_n)}{\mathrm{d}\theta_n} = -\epsilon p \sin(p\theta_n),$$

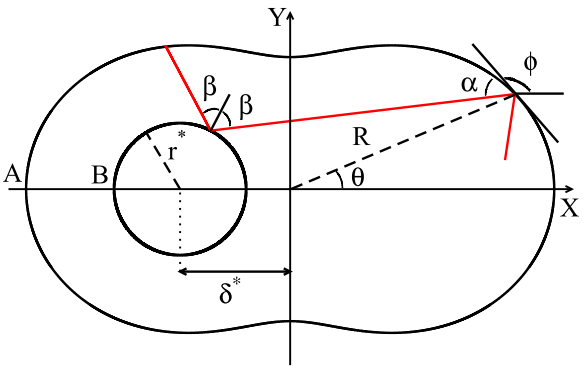

FIG. 1. Sketch for the external/internal boundaries and angles, for $p = 2$, $\epsilon = 0.3$ (oval billiard), $\delta^* = 0.5$, and $r^* = 0.3$. Locally negative curvatures in $\theta = \pi/2$ and $\theta = 3\pi/2$ are observed.

and for the elliptical billiard

$$\frac{dR(\theta_n)}{d\theta_n} = \frac{1}{2}\frac{\sin(2\theta)(b^2-a^2)}{\left[(b\cos\theta)^2+(a\sin\theta)^2\right]^{3/2}}.$$

Since there are no forces acting on the particle during the flight, its trajectory is a straight line given by

$$Y(\theta_{n+1}) - Y(\theta_n) = \tan(\mu_n)[X(\theta_{n+1}) - X(\theta_n))],$$

where $X(\theta_{n+1})$ and $Y(\theta_{n+1})$ are the coordinates of the collision new point and $\mu_n = \alpha_n + \phi_n$. The angle α_{n+1} in the collision is given by $\alpha_{n+1} = \phi_{n+1} - (\alpha_n + \phi_n)$. Using basic geometry, we end up with the mapping

$$T: \begin{cases} F(\theta_{n+1}) = Y(\theta_{n+1}) - Y(\theta_n) \\ \quad -\tan(\mu_n)[X(\theta_{n+1}) - X(\theta_n)] \\ \alpha_{n+1} = \phi_{n+1} - \mu_n, \end{cases} \tag{7}$$

which changes the variables θ_n and α_n to θ_{n+1} and α_{n+1}, in other words, $(\theta_{n+1}, \alpha_{n+1}) = T(\theta_n, \alpha_n)$. θ_{n+1} can be obtained numerically from the solution of $F(\theta_{n+1}) = 0$. The angle ϕ_{n+1} is obtained as $\phi_{n+1} = \arctan[Y'(\theta_{n+1})/X'(\theta_{n+1})]$, with X' and Y' given by Eqs. (5) and (6).

Mapping (7) describes the dynamics of the particle colliding with the external boundary. Now we introduce a scatterer in the billiard, indeed a circle of radius r^*, as shown in Fig. 1. δ^* is the distance between the zero mark and the center of the circle in the horizontal axis. For the oval billiard with $p = 2$ and for the elliptic billiard that we defined, the zero $(X, Y) = (0, 0)$ is in the center of the billiard.

When an internal scatterer is taken into account only one of two possible cases may happen: (i) a particle collides with the inner scatterer or (ii) the particle does not collide with the scatterer. Case (i) happens when $c_1 \le c_2$, where

$$c_1 = \sin(\theta_n - \alpha_n - \phi_n) - \frac{\delta^*}{R}\sin(\alpha_n + \phi_n)$$

and

$$c_2 = r^*/R(\theta_n).$$

While case (ii) is observed for $c_1 > c_2$.

The angle β in Fig. 1 has a sign convention. It is measured from the normal component of the inner circle to the straight line of the leaving particle, where it assumes negative value when particle is moving counterclockwise, and positive for clockwise and it is given by

$$\beta = \arcsin\left\{\frac{R(\theta_n)\sin(\theta_n - \alpha_n - \phi_n) - \delta^*\sin(\alpha_n + \phi_n)}{r^*}\right\}.$$

As soon as the particle collides with the inner scatterer, the position of the particle is $(X(\theta_n), Y(\theta_n)) = (X'_c, Y'_c)$, where $X'_c = r^*\cos(\gamma_n) - \delta^*$ and $Y'_c = r^*\sin(\gamma_n)$ with $\gamma_n = \pi - \beta + \alpha_n + \phi_n$. At such situation, the angle $\mu_n = \alpha_n + \phi_n + \pi - 2\beta$. Finally mapping (7) is then updated.

Fig. 2(a) shows a phase space for the oval billiard considering $r^* = \delta^* = 0$ and using $p = 2$ and $\epsilon = 0.1$ (only the external boundary is present). One can see that the phase space is mixed, containing Kolmogorov-Arnold-Moser (KAM) islands, a large chaotic sea and invariant spanning curves.

Fig. 2(b) shows a phase space for the oval billiard considering $p = 2$, $\epsilon = 0.1$, $\delta^* = 0$, and $r^* = 0.2$. One sees the two big islands in θ around $\pi/2$ and $3\pi/2$ cannot be observed because the inner circle destroyed them. We consider constant the value of $r^* = 0.2$ and move the position of the circle trying to observe what happens in the phase space. For $\delta^* = 0.0648$, as shown in Fig. 2(c), two KAM islands appear between the two red curves (we will explain how to obtain these curves later). These two islands approach each other until creating a saddle fixed point as shown in Fig. 2(d) for $\delta^* = 0.0828$. After increasing δ^*, an elliptic fixed point arises in the position $(\theta, \alpha) = (\pi, \pi/2)$ of the phase space (Fig. 2(d)). This phenomenon is called as direct parabolic bifurcation, therefore creating a fixed point from a saddle-center. This fixed point for $\delta^* = 0$ and $r^* = 0$ is unstable (hyperbolic fixed point), but the combination of parameters turned it an elliptic fixed point (stable). Increasing a little bit more the value of δ^* to 0.8 (see Fig. 2(f)) the fixed point in

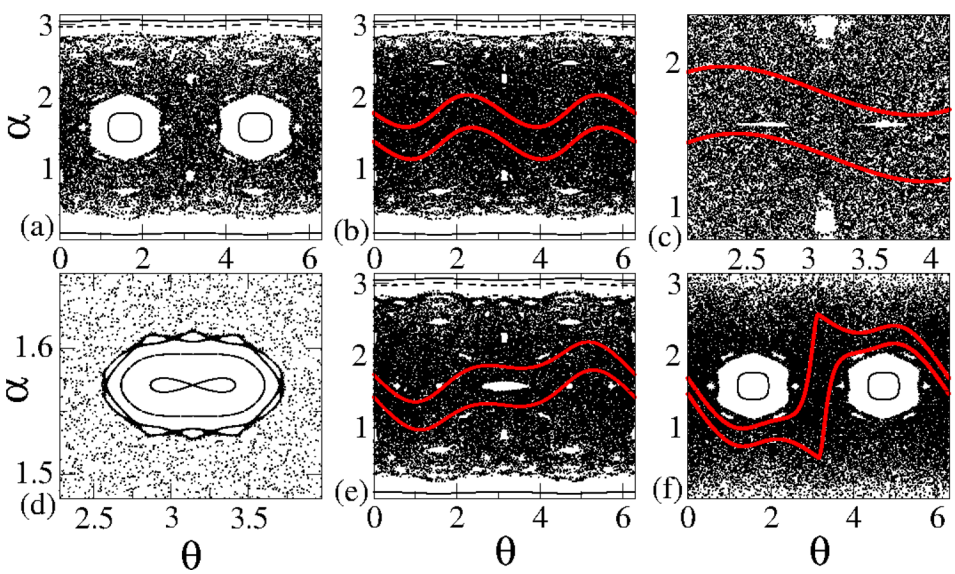

FIG. 2. Phase space for the oval billiard considering $p = 2$ and $\epsilon = 0.1$ and: (a) $r^* = \delta^* = 0$. For $r^* = 0.2$, the combination is (b) $\delta^* = 0$; (c) $\delta^* = 0.0648$; (d) $\delta^* = 0.0828$; (e) $\delta^* = 0.2538$; (f) $\delta^* = 0.8$. Between the two red lines, the particle suffers collisions with the inner circle. The lines are plotted by the expressions of α_{m1} and α_{m2} (see Eqs. (8) and (9)).

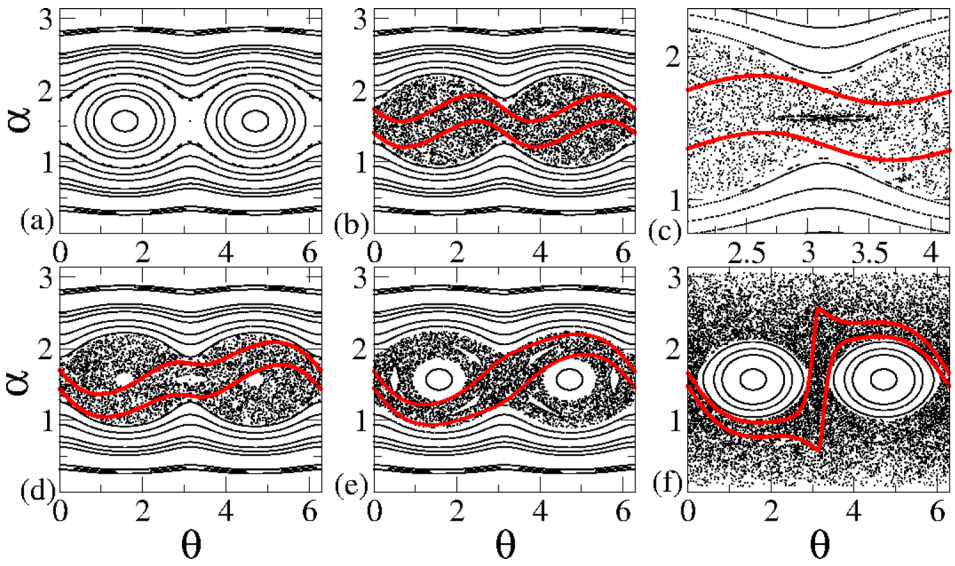

FIG. 3. Phase space for the elliptic billiard considering $a=1.2$ and $b=1$ and (a) $r^*=\delta^*=0$. For $r^*=0.2$, the combination is (b) $\delta^*=0.002$; (c) $\delta^*=0.152$; (d) $\delta^*=0.316$; (e) $\delta^*=0.548$; and (f) $\delta^*=0.998$. Between the two red lines, the particle suffers collisions with the inner circle. The lines are plotted by the expressions of α_{m1} and α_{m2} (see Eqs. (8) and (9)).

$(\theta,\alpha)=(\pi,\pi/2)$ becomes unstable. Also the invariant spanning curves were destroyed.

To visualize the region in the phase space where a collision with the internal circle happens, we have to obtain the angles α_{m1} and α_{m2} which define the limits of this region. These angles are

$$\alpha_{m1}=(\theta-\alpha'_{m1}-\phi)\mod(\pi), \tag{8}$$

$$\alpha_{m2}=(\theta-\alpha'_{m2}-\phi)\mod(\pi), \tag{9}$$

where $\alpha'_{m1}=(A_2+A_3)/A_4$, $\alpha'_{m2}=(-A_2+A_3)/A_4$ and the auxiliary variables are given by

$$A_1=\frac{\delta^*\cos(\theta)}{R(\theta)},$$

$$A_2=r^*(1+A_1),$$

$$A_3=\delta^*\sin\theta\sqrt{1+\frac{(\delta^*)^2-(r^*)^2}{[R(\theta)]^2}+2A_1},$$

$$A_4=R(\theta)+\delta^*\left[2\cos(\theta)+\frac{\delta^*}{R(\theta)}\right].$$

The angles α_{m1} and α_{m2} as a function of θ are shown as the red curves in Figs. 2(b), 2(c), 2(e), and 2(f). The region between the two curves represents the conditions in which collisions with the inner circle happen.

Now we obtain the phase space for the elliptic billiard. To start with, we consider the radius of the inner circle equal to zero ($r^*=0$), and the results are shown in Fig. 3(a). The phase space is regular, containing only periodic and quasi-periodic orbits. After introducing a scatterer with $r^*=0.2$ and $\delta^*=0.002$, the phase space changes and as shown in Fig. 3(b), a chaotic sea appears near $\alpha=\pi/2$. Increasing the value of δ^* to 0.152 (Fig. 3(c)), we can see the beginning of the direct parabolic bifurcation that ends with the creation of the elliptical fixed point in $\theta=\pi$, as shown in Fig. 3(d) for $\delta^*=0.316$. When setting $\delta^*=0.548$ (Fig. 3(e)), an inverse parabolic bifurcation occurred, and the fixed point in $\theta=\pi$ now became unstable. Finally, for $\delta^*=0.998$ (Fig. 3(f)), the invariant spanning curves were destroyed. As conclusion, we observed that the direct and inverse parabolic bifurcations happen for both elliptical and oval billiards.

A. Linear stability of some fixed points

In this subsection, we study the linear stability of some fixed points trying to better understand the dynamics of the billiard.

The control parameters where a direct parabolic bifurcation and hence a creation of fixed point from a saddle center happens are shown in Figs. 4(a) and 4(b) for $p=2$. This kind of bifurcation can be observed, for example, in Figs. 2(c)–2(e), where an elliptical fixed point arose. For Fig. 4(a), it is shown δ^* vs r* for different values of ϵ. Figure 4(b) shows δ^* as function of ϵ for three different values of r^*. Observing Figs. 2(e) and 2(f), we see the fixed point in $\theta=\pi$ is no longer elliptic when δ^* is increased. This happens because the occurrence of an inverse parabolic bifurcation and the fixed point becomes unstable. Figure 4(c) shows the value of the control parameters in which such bifurcations occur. As one can see, apparently, it does not depend on the control parameter r^*.

We show the numerical results for the elliptic billiard considering $b=1$. Figure 4(d) shows a plot of δ^* vs r* for three different values of the control parameter a where a direct parabolic bifurcation happens. Figure 4(e) shows a plot of δ^* vs a now considering three values of r^*. Finally, Fig. 4(f) shows the results for the inverse parabolic bifurcation, where the value of δ^* does not depend on the values of r^*.

A method to explore analytically the results found here is to study the linear stability of the fixed points. To compute this, it is convenient to introduce Greene's residue R and its complement $\bar{R}$, which are defined by[7]

$$\bar{R}=1-R=(2+\mathrm{tr}_j^2)/4, \tag{10}$$

where $\mathrm{tr}_j^{(2)}=\mathrm{tr}\prod_{i=1}^{j}\mathbf{M}_i^{(2)}\mathbf{K}_i^{(2)}$. $\mathbf{K}^{(2)}$ is the linearised reflection matrix. The stability is split up into contributions from

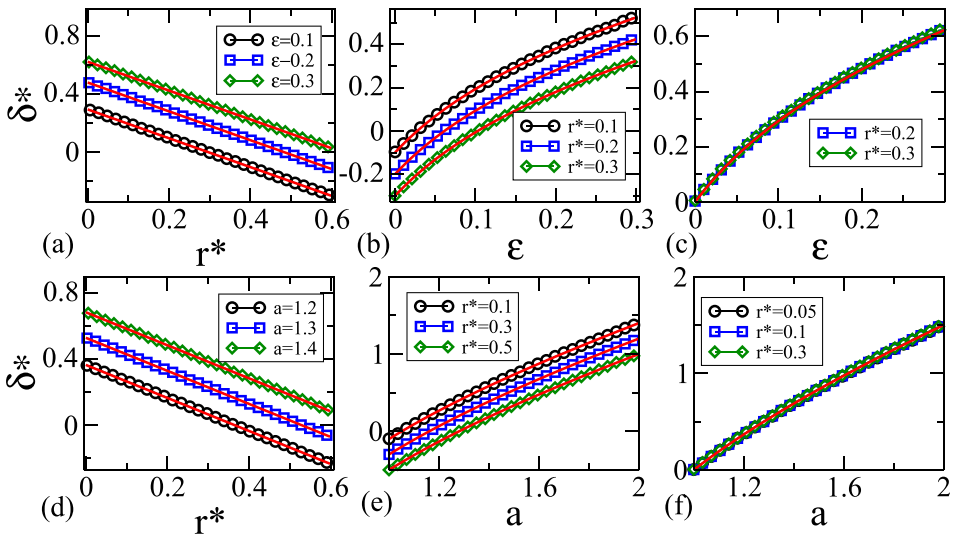

FIG. 4. For the oval billiard with $p=2$, we have in (a) and (b) the value of the control parameters in which we have a direct parabolic bifurcation, where (a) shows δ^* vs r^* considering three different values of ϵ and (b) exhibits δ^* vs ϵ for three different values of r^*. In (c), we have the control parameters in which we have an inverse parabolic transition. In (d)–(f), we have the results for the elliptic billiard, where (d) and (e) show the results for the direct parabolic bifurcation and the item (f) shows the inverse parabolic bifurcation. The red lines represent the analytic results obtained.

the reflection $\mathbf{K}^{(2)}$ and from the free motion $\mathbf{M}^{(4)}$. j is the period of the orbit.[7]

For an orbit starting from $\theta=\pi$, one shows that $tr^{(2)}_{j=2}$ (period two orbit) can be written as

$$\cdots\begin{pmatrix}1 & \tau\\ 0 & 1\end{pmatrix}\begin{pmatrix}-1 & 0\\ 2\kappa_1/\eta_1 & -1\end{pmatrix}\begin{pmatrix}1 & \tau\\ 0 & 1\end{pmatrix}\begin{pmatrix}-1 & 0\\ 2\kappa_2/\eta_2 & -1\end{pmatrix}\cdots, \tag{11}$$

where η_1 and η_2 are, respectively, the normal component of the velocity in the collision points A and B (see Fig. 1). For the static boundary case, we know that the velocity is constant and we consider $\eta_1=\eta_2=1$. κ_1 is the curvature in the collision point A, and $\kappa_2=-1/r^*$ is the curvature in the point B of the inner circle. τ in our simulation represents the time to travel the distance AB. Multiplying the matrices in Eq. (11), we obtain that $tr^{(2)}_{j=2}=-2(-r^*+2\tau\kappa_1 r^*-2\tau+2\tau^2\kappa_1)/r^*$, where after combining with Eq. (10) we obtained that

$$R=\frac{\tau[\kappa_1(r^*+\tau)-1]}{r^*}. \tag{12}$$

For billiards, the curvature κ_2 can be obtained using the following expression:[30]

$$\kappa(\theta)=\frac{X'(\theta)Y''(\theta)-X''Y'(\theta)}{[X'^2(\theta)+Y'^2(\theta)]^{3/2}},$$

where $X''=d(X')/d\theta$ and $Y''=d(Y')/d\theta$. X' and Y' were previously defined in Eqs. (5) and (6).

To better visualize the findings, first we show the results for the oval billiard, and after that the results for the elliptic billiard are presented.

1. Results for the oval billiard

As mentioned before, τ indirectly is the measure of the distance $\overline{AB}$ when $\theta=\pi$, and its value for the oval billiard is equal to

$$\tau=R_a-(\delta^*+r^*), \tag{13}$$

where in this case $R_a=R(\theta=\pi)=1+\epsilon\cos(p\pi)$. For the same angle $\theta=\pi$, the curvature is equal to

$$\kappa_1=\frac{2\left[\epsilon p\sin(p\pi)\right]^2-R_a\left[\epsilon p^2\cos(p\pi)+R_a\right]}{\left\{\left[\epsilon p\sin(p\pi)\right]^2+R_a\right\}^{3/2}}. \tag{14}$$

Solving Eq. (12) for $R=1$, the control parameter δ^* is equal to

$$\delta^*=-\frac{5r^*\epsilon-3\epsilon-\epsilon\cos(p\pi)+\epsilon^2-5\epsilon^2\cos(p\pi)+r^*}{5\epsilon+1}, \tag{15}$$

where this equation gives the parameter where a direct parabolic bifurcation happens.

Now solving Eq. (12) for $R=0$, we have that

$$\delta^*=\frac{\epsilon\left[5\epsilon\cos(p\pi)+\cos(p\pi)+3-\epsilon\right]}{5\epsilon+1}, \tag{16}$$

where an inverse parabolic transition happens, i.e., the elliptical fixed point becomes unstable. As one can see, the value of δ^* in this case does not depend on r^*, and it is only a function of ϵ.

For a particular case, when $p=2$ (convex oval billiard) the curvature for $\theta=\pi$ is given by

$$\kappa_1=\frac{5\epsilon+1}{(1+\epsilon)^2}. \tag{17}$$

The direct parabolic bifurcation ($R=1$) happens at

$$\delta^*=-\frac{5r^*\epsilon+r^*-4\epsilon-4\epsilon^2}{5\epsilon+1}, \tag{18}$$

and the inverse parabolic bifurcation ($R=0$) is obtained for

$$\delta^*=\frac{4\epsilon(1+\epsilon)}{5\epsilon+1}. \tag{19}$$

We notice that Eqs. (19) and (18) have the same expression for $r^*=0$.

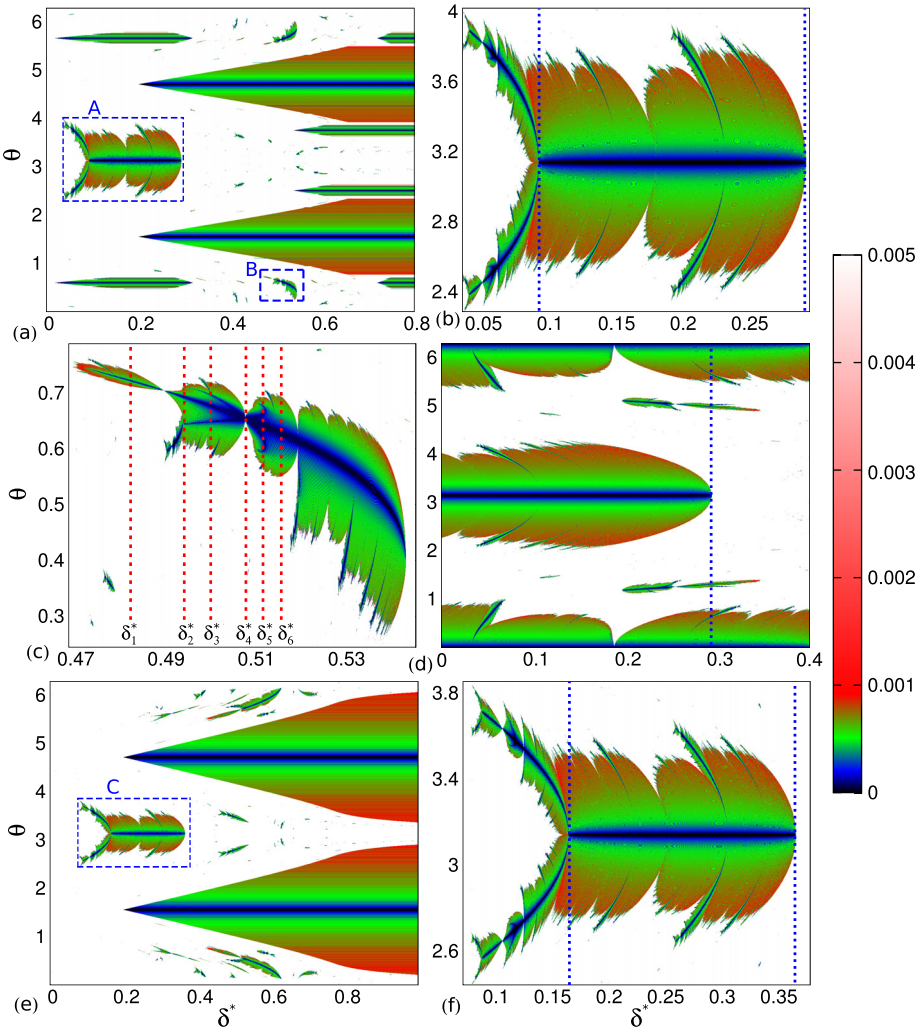

FIG. 5. Conservative generalized bifurcation diagrams considering θ as a function of δ^*. In (a)–(c), an oval billiard is considered with $p=2$ and $\epsilon=0.1$, where the radius of the inner circle equal to $r^*=0.2$. In (d), the same oval billiard is considering but now for $r^*=0.7$. In (e) and (f), the results for an elliptical billiard considering $a=1.2$ and $b=1$ are shown for $r^*=0.2$. Here, $\delta_1^*=0.4827$, $\delta_2^*=0.4947, \delta_3^*=0.5005, \delta_4^*=0.5083$, $\delta_5^*=0.5121$, and $\delta_6^*=0.5161$.

The analytical results presented above are plotted in Figs. 4(a)–4(c) as the red continuous line. As one can see, the numerical and analytical results are in good agreement.

For the circle billiard with $\epsilon=0$, the direct and inverse parabolic bifurcation occurs, respectively, for $\delta^*=-r^*$ and $\delta^*=0$.

2. Results for the elliptic billiard

For the elliptic billiard, the distance $\overline{AB}$ and consequently the time τ for $\theta=\pi$ is given by

$$\tau = a-(\delta^*+r^*). \tag{20}$$

The curvature in the collision point A is given by

$$\kappa_1 = \frac{a}{b^2}. \tag{21}$$

Solving Eq. (12) for $R=1$, we have

$$\delta^* = \frac{a^2-b^2-ar^*}{a}, \tag{22}$$

which characterizes the parameter of direct parabolic bifurcation. For $R=0$, Eq. (12) assumes the following expression:

$$\delta^* = \frac{a^2-b^2}{a}, \tag{23}$$

giving an inverse parabolic transition. The expression for δ^* does not depend on the control parameter r^*.

Now for the circle billiard with $a=b=1$, the direct and inverse parabolic perturbations occur, respectively, for $\delta^*=-r^*$ and $\delta^*=0$, which confirms the results obtained for the oval billiard with $\epsilon=0$. The analytical results obtained here are shown in Figs. 4(d)–4(f) as the red lines, confirming a good agreement between theory and simulation.

B. Conservative generalized bifurcation diagram

Now we study the Lyapunov exponents in order to obtain the conservative generalized bifurcation diagrams. One can use the Lyapunov exponents to characterize the chaotic sea. They show great applicability as a practical tool that can quantify the average expansion or contraction rate for a small volume of initial conditions. As discussed in Ref. 31, the Lyapunov exponents are defined as

$$\lambda_j = \lim_{n\to\infty}\frac{1}{n}\ln|\Lambda_j|, \quad j=1,2, \tag{24}$$

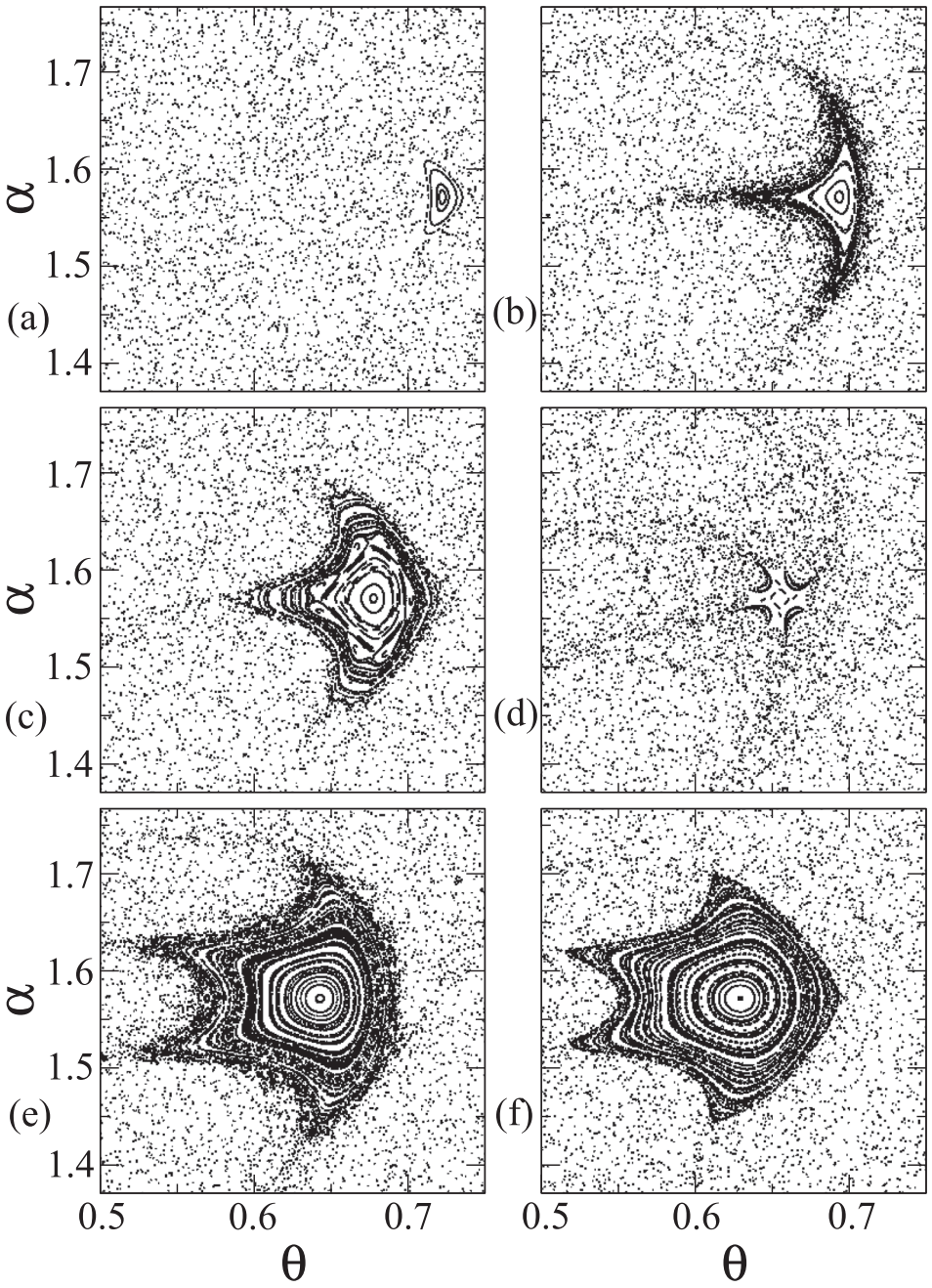

FIG. 6. Phase space for fixed values of $r^* = 0.2$, $p = 2$, $\epsilon = 0.1$, and $e = 0$ and the values of δ^* are equal to (a) $\delta_1^* = 0.4827$; (b) $\delta_2^* = 0.4947$; (c) $\delta_3^* = 0.5005$; (d) $\delta_4^* = 0.5083$; (e) $\delta_5^* = 0.5121$; and (f) $\delta_6^* = 0.5161$.

where Λ_j are the eigenvalues of $M = \prod_{i=1}^{n} J_i(\theta_i, \alpha_i)$ and J_i is the Jacobian matrix evaluated over the orbit (θ_i, α_i). If at least one of the λ_j is positive, then the orbit is classified as chaotic. Therefore, we define λ as the larger value of the λ_j.

Given how to obtain the Lyapunov exponents, we now obtain the CGBD. We know that the Lyapunov exponents are defined in the limit of $n \to \infty$. However, here in the CGBD simulations, it is necessary to consider the finite Lyapunov exponents, i.e., the maximum n needs to be a finite value. We consider in our simulations $n = 10^4$. To do so, we start different orbits with $\alpha = \pi/2$ and $\theta \in [0, 2\pi)$, see Fig. 2. For such a situation, we plot θ as function of the control parameters and the color represents the finite Lyapunov exponents. In Figs. 5(a)–5(c), we have a plot of θ vs δ^* considering an oval billiard with $p = 2$, $\epsilon = 0.1$, and $r^* = 0.2$. For Fig. 5, we considered as colors a customized pallet that considers for $\lambda < 0.0001$ the color black, and a continuous black to blue scheme color in the interval 0.0001 to 0.0003, blue to green between 0.0003 until 0.0006, green to red in the interval 0.0006 to 0.001, and finally red to white in the interval 0.001 to 0.005. For $\lambda > 0.001$, the color white is used. In Fig. 5(a), the periodic orbits are characterized as the low values of λ, which correspond to the black (blue) regions. The results for an enlargement in the region A is shown in Fig. 5(b), where the two dotted lines represent the analytical results obtained in Eqs. (18) and (19). The values obtained are $\delta^* \cong 0.09333$ for $R = 1$ and $\delta^* \cong 0.29333$ for $R = 0$. As confirmed in Fig. 5(b), for δ^* less than 0.09333, a period 2 elliptical fixed point becomes a period 1 after a direct parabolic bifurcation. The inverse parabolic bifurcation is also highlighted in Fig. 5(b), where a period 1 fixed point vanishes for $\delta^* > 0.09333$. Figure 5(c) shows an enlargement in region C of Fig. 5(a).

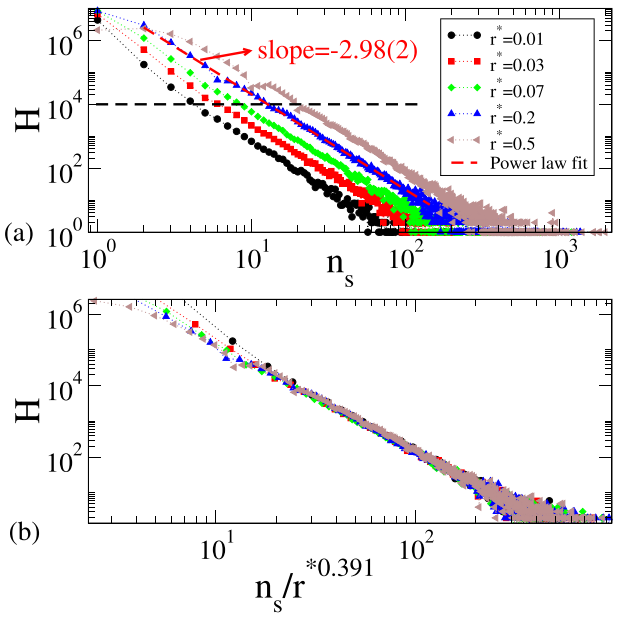

FIG. 7. Histogram H_1 vs the number of iterations n for different values of r^* in a cusp ($p=2$ and $\epsilon=0.01$). In (b), all curves collapsed after a properly rescale $(n_s \to n_s/(r^*)^{0.391})$, therefore, showing a scaling invariance.

Figure 5(d) shows the results of CGBD for the oval billiard, but now considering the radius of the inner circle equals to $r^* = 0.7$. The analytical result is shown as the dashed line.

Figures 5(e) and 5(f) show the results for an elliptical billiard, with $a=1.2$ and $b=1$. The parameter $r^* = 0.2$ is chosen and again δ is varied. Figure 5(f) is an enlargement of region C of Fig. 5(e). As one can see, the numerical and analytical results are in good agreement.

Here, we obtained analytically the first duplication of period; however, the CGBD can show other bifurcations. As we observed in Fig. 5(c), apparently, we have different behaviors when varying δ. Figs. 6(a)–6(f) show some phase space for the values of δ, respectively, equal to $\delta_1^* = 0.4827$, $\delta_2^* = 0.4947$, $\delta_3^* = 0.5005$, $\delta_4^* = 0.5083$, $\delta_5^* = 0.5121$, and $\delta_6^* = 0.5161$. In Fig. 6(a), we have apparently only one KAM islands. When increasing the value of δ, different bifurcations occur, and for $\delta \to \delta_6^*$ again we have only one KAM island. Our intention here is just to show that the CGBD can be used as a tool to observe different kinds of bifurcation.[26]

C. Number of successive iterations for a cusp (considering the oval billiard)

Here, the results when considering the number of successive iterations (n_s) for $X < -\delta^*$ are shown. Basically, $X < -\delta^*$ is the region in the left of the center of the inner circle shown in Fig. 1. Only the oval circle is considered in the simulations. It is just a start to understand the complex behavior that occurs when a cusp is present. A cusp is observed, when the inner circle touches the external boundary, leading the distance AB to be zero. Indeed, it happens when $\delta^* = 1 + \epsilon - r^*$.

Figure 7(a) shows a histogram H for the number of successive iterations for $X < -\delta^*$ in a time n and for different values of r^*. In these simulations, we considered $p=2$, $\epsilon = 0.01$, $\alpha_0 = 2$, and $\theta_0 = 0.1$. In a cusp, the histogram H is described by a power law with slope -3. Following the dashed straight line at $H = 10^4$, one can see that the higher value of r^* the higher is the value of n_s. n_s vs r* was computed and as result $n_s \propto r^{\chi}$ was found. Simulations for different values of ϵ were performed and the results are shown in Table I. As observed, the average slope χ obtained is about 0.391 and apparently does not depend on ϵ. We propose a rescale in the horizontal axis of Fig. 7(a) $(n_s \to n_s/r^{0.391})$, and the result is shown in Fig. 7(b). The histogram H seems to be scaling invariant.

TABLE I. Slope χ when considering different values of the control parameters ϵ for the oval billiard with $p=2$.

	$\epsilon=0$	$\epsilon=0.1$	$\epsilon=0.2$	$\epsilon=0.3$
χ	0.394(9)	0.391(6)	0.408(8)	0.39(1)

III. SUMMARY AND CONCLUSIONS

We studied some dynamical properties for classical particles in a billiard, where the external boundary is an elliptic, oval, or circle billiard and an inner circle was introduced. The billiard here proposed is a generalization (explored for the first time) of the annular billiard; this one is interesting for understanding MUPOs and their role in the boundary between regular and chaotic regions in both classical, quantum, and experimental systems. Considering the outer boundary as an oval billiard is worth because an obstacle is introduced in a mixed boundary. The model was carefully obtained and the conditions leading to collisions with the scatterer were obtained. We showed that the billiard presents direct and inverse parabolic bifurcations for some special combinations of control parameters when $\theta = \pi$, and the results were confirmed analytically and numerically. We show some examples of conservative generalized bifurcation diagrams, particularly a link with the direct and inverse parabolic bifurcations. We also observed that it is possible to use the conservative generalized bifurcation diagrams as a tool to find some more complex bifurcations as made in Ref. 26. In the last part of the paper, histograms for the number of successive iterations in a cusp are studied. These histograms have a power law behavior with slope of -3, and they are scaling invariant when changing the radius of the scatterer. It is important to mention that the cusps here presented are completely new, because only two dispersing or one dispersing and one flat boundary can be observed in the literature.[27–29] The results here presented are a first step trying to understand the complicated dynamic of the billiard here proposed. More studies are necessary to understand some phenomena, including the role of MUPOs and stickiness both classically and quantum mechanically.

ACKNOWLEDGMENTS

D.R.C. acknowledges Brazilian agency FAPESP (2010/52709-5, 2012/18962-0, and 2013/22764-2). E.D.L. thanks to CNPq, FUNDUNESP and FAPESP (2012/23688-5), Brazilian agencies. J.A.O. thanks to FAPESP (2014/18672-8) and PROPe/FUNDUNESP (Brazilian agencies). We would like to

thank Vitaly Fain for the valuable discussions and a careful reading of this paper. This research was supported by resources supplied by the Center for Scientific Computing (NCC/GridUNESP) of the São Paulo State University (UNESP).

[1]E. G. Altmann, J. C. Leitão, and J. V. Lopes, Chaos **22**, 026114 (2012).
[2]J. Liss, B. Liebchen, and P. Schmelcher, Phys. Rev. E **87**, 012912 (2013).
[3]J. Nagler *et al*., Phys. Rev. E **75**, 046204 (2007).
[4]B. Castaldi, R. E. de Carvalho, C. V. Abud, and A. P. Mijolaro, Phys. Rev. E **89**, 012916 (2014).
[5]E. G. Altmann, J. S. E. Portela, and T. Tél, Phys. Rev. Lett. **111**, 144101 (2013).
[6]G. D. Birkhoff, *Dynamical Systems* (American Mathematical Society, Providence, RI, 1991).
[7]H. R. Dullin, Nonlinearity **11**, 151–173 (1998).
[8]E. G. Altmann, T. Friedrich, A. E. Motter, H. Kantz, and A. Richter, Phys. Rev. E **77**, 016205 (2008).
[9]L. A. Bunimovich and Y. Sinai, Commun. Math. Phys. **78**, 479 (1981).
[10]A. E. Hartl, B. N. Miller, and A. P. Mazzoleni, Phys. Rev. E **87**, 032901 (2013).
[11]X. Yu and Y. Zhang, Chaos **23**, 013107 (2013).
[12]I. A. Kotelnikov, S. S. Popov, and M. Romé, Phys. Rev. E **87**, 013111 (2013).
[13]V. Gelfreich, V. Rom-Kedar, and D. Turaev, Chaos **22**, 033116 (2012).
[14]E. G. Altmann, J. S. E. Portela, and T. Tél, Rev. Mod. Phys. **85**, 869–918 (2013).
[15]A. K. Karlis, F. K. Diakonos, C. Petri, and P. Schmelcher, Phys. Rev. Lett. **109**, 110601 (2012).
[16]D. R. da Costa, M. R. Silva, and E. D. Leonel, Commun. Nonlinear Sci. Numer. Simul. **19**, 842–850 (2014).
[17]M. R. Silva, D. R. da Costa, and E. D. Leonel, J. Phys. A **45**, 265101 (2012).
[18]N. Saitô *et al*.. Physica D **5**, 273–286 (1982).
[19]R. E. de Carvalho, F. C. Souza, and E. D. Leonel, Phys. Rev. E **73**, 066229 (2006).
[20]R. E. de Carvalho and A. P. Mijolaro, Phys. Rev. E **70**, 056212 (2004).
[21]R. E. de Carvalho, F. C. de Souza, and E. D. Leonel, J. Phys. A **39**, 3561–3573 (2006).
[22]C. Dembowski, H.-D. Gräf, A. Heine, R. Hofferbert, H. Rehfeld, and A. Richter, Phys. Rev. Lett. **84**, 867 (2000).
[23]R. Hofferbert, H. Alt, C. Dembowski, H.-D. Gräf, H. L. Harney, A. Heine, H. Rehfeld, and A. Richter, Phys. Rev. E **71**, 046201 (2005).
[24]F. Lenz, F. K. Diakonos, and P. Schmelcher, Phys. Rev. Lett. **100**, 014103 (2008).
[25]M. V. Berry, Eur. J. Phys. **2**, 91–102 (1981).
[26]C. Manchein and M. W. Beims, Phys. Lett. A **377**, 789 (2013).
[27]N. Chernov and R. Markarian, Commun. Math. Phys. **270**, 727–758 (2007).
[28]P. Bálint, N. Chernov, and D. Dolgopyat, Commun. Math. Phys. **308**, 479–510 (2011).
[29]P. Bálint and I. Melbourne, J. Stat. Phys. **133**, 435–447 (2008).
[30]D. F. M. Oliveira and E. D. Leonel, Commun. Nonlinear Sci. Numer. Simul. **15**, 1092–1102 (2010).
[31]J. P. Eckmann and D. Ruelle, Rev. Mod. Phys. **57**, 617 (1985).